Electronic Supplementary Material (ESI) for Nanoscale.

Supplementary Information for

Highly Efficient Bifunctional Oxygen Reduction/Evolution Activity in a Non-Precious Nanocomposite Derived from Tetrazine-COF

Soumyabrata Roy,[1,2] Subbareddy Mari,[1,2] Manoj Kaja Sai,[1,2] Saurav Ch. Sarma,[1,2] Shreya Sarkar,[1,2] and Sebastian C. Peter[1,2]

[1]New Chemistry Unit, Jawaharlal Nehru Centre for Advanced Scientific Research, Bangalore, India
[2]School of Advanced Materials, Jawaharlal Nehru Centre for Advanced Scientific Research, Bangalore 560 064, India

1. Experimental section

1.1 Synthesis

All the chemicals and reagents were used as such, without any further purification. 1, 3, 5-tricyanobenzene (TCB) organic ligand was synthesized by following the reported method.[1]

1.1.1 Benzene-1, 3, 5-tricarbonyltrichloride

1, 3, 5 tricarboxylic acid (10 g) taken in a 100 ml round-bottom flask, thionyl chloride ($SOCl_2$, 10 ml) and DMF (3 drops) were added. The entire solution was refluxed for overnight. The unreacted $SOCl_2$ was evaporated by using rotovapour. The obtained product was white solid.

1.1.2 1, 3, 5-Tricarbamoylbenzene

Benzene-1, 3, 5-tricarbonyltrichloride (8 g, 30 mmol) was stirred cautiously with aqueous concentrated ammonia solution (75 ml) in a 250 ml round-bottom flask. Once the vigorous exothermic reaction had subsided, the resulting dense white precipitate was stirred for another 5h. The solid was then filtered, washed with ethanol (3×25 ml) and dried at 80 ^oC. The product was an amorphous white solid.

1.1.3 1, 3, 5-Tricyanobenzene

1,3,5-Tricarbamoylbenzene (4.6 g, 22.2 mmol) was stirred in dimethylformamide (35 ml) and thionyl chloride ($SOCl_2$, 6 ml) added to the suspension over 1h maintaining the temperature at 60 ^oC. Stirring at this temperature for 6 h during which time complete dissolution occurred. The resulting solution was poured into dilute HCl (100 ml) to decompose unreacted $SOCl_2$, giving a dense white precipitate. This solid was filtered off, washed with water until neutral and dried at 120 ^oC for 14h. Crystallization from ethanol and acetone yielded the colorless product, further dried at 100 ^oC.

1.1.4 TZA-COF

TZA-COF was synthesized by adopting the reported method by varying the organic ligand.[2] In a typical process, 1, 3, 5-tricyanobenzene (120 mg, 0.71 mmol) and sulfur (450 mg, 9.37 mmol) were dissolved in ethanol (10 mL) in a 25 mL round flask, followed by the addition of hydrazine (10 mL). The reaction mixture was magnetically stirred and heated to reflux for 1 day. After cooling, the solvent was removed by filtration and the resulting light yellow solid was washed thoroughly with hydrazine hydrate, water, and ethanol. The collected filtrate was done soxhlet extraction for 4 days by changing fresh tetrahydrofuran (THF) every day. (Yield: 65% ~ 70%).

1.1.5 Graphene Oxide (GO)

Graphene oxide (GO) was synthesized from graphite powder by a modified Hummer's method.[3] Further reduction of GO to form rGO was carried out by a solution method which is performed in the presence of hydrazine hydrate at 90 ºC for 24 h.

1.1.6 TZA COF-rGO hybrids (5, 10 and 20 mg)

The composite hybrids of **COF-rGO** were synthesized by the same procedure as followed for COF synthesis. The only difference is that the COF precursors were dissolved directly in the uniform dispersion of GO (at different concentrations, i.e 5, 10 and 20 mg termed as **COF-rGO(5), COF-rGO(10), and COF-rGO(20)**. Reduction of GO to rGO occurred during the formation of COF.

1.1.7 COF-rGO(10)-Co(20)

TZA-COF-rGO-Co(20) hybrid was synthesized by wet impregnation method followed by $NaBH_4$ reduction. Initially, cobalt impregnation was done on **COF-rGO(10)** (60 mg) by a wet impregnation method in which $Co(NO_3)_2.6H_2O$ (59.8 mg 20 wt%) used as cobalt source. The obtained cobalt impregnated hybrid was reduced by using sodium borohydride (120 mg) in water (25 mL) by ultrasonication for 3h.

1.1.8 Co@NC-600

Co@NC-600 was synthesized by using **COF-rGO(10)-Co(20)** (20 wt%) hybrid. **COF-rGO(10)-Co(20)** (20 wt%) (50mg) was taken in a 13 mm glass tube and sealed by applying vacuum. The sealed glass tube was placed in a tubular furnace at 600 ºC for 6 h and cooled naturally to the room temperature. The obtained **Co@NC-600** product was in black color with a yield of 20 mg.

1.2 Characterization

1.2.1 PXRD measurements

The PXRD measurements at room temperature were carried out on a Rigaku miniflex X-ray diffractometer and BrukerD8 Discover diffractometer using Cu-*Kα* as the X-ray source (λ = 1.5406 Å). The instrument is equipped with a position sensitive detector in the angular range $20^o \leq 2\theta \leq 90^o$ with the step size 0.02^o and scan rate of 1 sec/step calibrated against corundum standard. The experimental patterns were compared to the pattern simulated from the database. Synchrotron PXRD data was collected at BL-18B beamline at Photon Factory, KEK, Japan using X-ray wavelength of 0.9782 Å. The energy of the beam was set by a Si(111) double crystal monochromator, which was cross checked with a Si (640b NIST) standard. Different possible extended structure of COF were designed using Gauss View 6.0.16 program suite and corresponding PXRD patterns were generated using the Mercury-CCDC software. Simulated powder patterns were then matched with the experimentally observed data to find the best fitted model.

1.2.2 Transmission electron microscopic imaging

TEM images and selected area electron diffraction patterns were collected using a JEOL JEM-2010 TEM instrument and color mapping was done in TECHNAI. The samples for these measurements were prepared by sonicating the nanocrystalline powders in ethanol and drop-casting a small volume onto a carbon-coated copper grid.

1.2.3 X-ray photoelectron spectroscopy

XPS measurement was performed on powdered samples of **COF-rGO-Co** & **Co@NC-600** in an Omicron Nanotechnology spectrometer using a Mg−*kα* (λ = 1253.6 eV) X-ray source with a relative composition detection better than 0.1%.

1.2.4 Raman spectroscopy

Raman spectra were collected on powdered samples in the backscattering geometry using a 632 nm HeNe laser with a Jobin Yvon LabRam HR 800 spectrometer.

1.2.5 UV-Vis absorption spectra

Absorption spectra were recorded in the UV−VIS region using PerkinElmer Lambda750 UV instrument. The spectra were collected in the reflectance mode in the range of 200−800 nm on solid powdered samples using $BaSO_4$ as the reference. The powdered samples were put in a circular sample holder with a transparent quartz window. All the sample spectra were corrected with $BaSO_4$ as the reference.

1.2.6 Thermogravimetric analysis

TGA analysis of the samples (**TZA-COF** & **COF-rGO(10)**) were done using a Mettler TGA 850 under nitrogen atmosphere between 25 and 850 °C at a heating rate of 5 °C min^{-1}. The samples showed similar thermogravimetric behaviour with sequential decays of solvents, followed by degradations of the organic ligands. A weight loss of (1.6%) happened between 250 and 350 °C. The loss of organic ligands broadly occurred in two steps between 350 and 450 °C (~4-5%) and between 450 and 800 °C (7-14%).

1.2.7 Scanning electron microscopy and EDAX/ Elemental analysis

The EDX measurement was performed using FEI NOVA NANOSEM 600 scanning electron microscope equipped with an energy-dispersive X-ray spectroscopy (EDAX) instrument (Bruker 129 eV EDAX instrument). Data was acquired by using an accelerating voltage of 20 kV and typical time taken for data accumulation is 100 s. The elemental analyses were performed using the P/B-ZAF standardless method (where, P/B = peak to background model, Z = atomic no. correction factor, A = absorption correction factor and F = fluorescence factor) for C, N, O, Co at multiple areas on the sample coated Si wafer.

1.2.8 Adsorption Measurements

Adsorption isotherms of N_2 at 77 K & CO_2 at 273 K were performed on the desolvated samples (at 150 ºC) using a QUANTACHROME QUADRASORB-SI analyzer. About 50 mg of each sample was degassed at 150 °C under 10^{-1} Pa vacuum for about 12 h before the measurements. 99.999% (UHP) pure helium gas was used to measure the dead volume of the sample cell. Adsorbed gas amounts were calculated from the pressure difference (Pcal − Pe), where Pcal is the calculated pressure with no gas adsorption and Pe is the observed equilibrium pressure. All the operations were automatic and computer-controlled.

1.3 Electrochemical measurements

All the electrochemical measurements were performed by using CHI 760E electrochemical workstation in three electrode configuration. Hg/HgO was used as reference electrode and platinum coil as counter electrode. All the potentials reported here were corrected to reversible hydrogen electrode (RHE).

Process for RHE conversion: The calibration of Hg/HgO electrode was performed in a standard three-electrode system with polished Pt wires as the working and counter electrodes, and the Hg/HgO as the reference electrode. Electrolytes are continuously purged and saturated with high purity H_2. Cyclic voltammetry (CV) is then run at a scan rate of 5 $mVsec^{-1}$, and the average of the potential, from both the sweeps, at which the current crossed zero is taken to be the thermodynamic potential for the hydrogen electrode reactions. For example, in 0.1 M KOH, the zero current point is at -0.936 V, so $E_{(RHE)} = E_{(Hg/HgO)} + 0.936$ V.

Electrocatalytic activity was studied in O_2 saturated 0.1M KOH using rotating disk electrode (RDE) for ORR and N_2 saturated 0.5M KOH for OER. Catalyst slurry was prepared by dispersing 1.6 mg of the catalysts and 0.4 mg vulcan in 200ul of 1:3 IPA and H_2O mixture. This dispersion was sonicated well to obtain homogenous catalyst slurry. ORR and OER studies were performed on rotating disk electrode (RDE), fitted with glassy carbon of area 0.0706 cm^2. Working electrodes were prepared by drop casting 10 µl of catalyst slurry on RDE and dried under infrared lamp to obtain uniform coating. 5 µl of nafion (1wt%) was casted on it just before drying. Here Pt and Pd were used as reference benchmark catalysts for ORR, while IrO_2 was used as the same for OER. 20 wt% Pt-C and 20 wt% Pd-C were obtained from Sigma Aldrich. 2mg of them were dispersed in 200ul of 1:3 IPA and H_2O mixture and sonicated well to get homogenous slurry. 10 µl of this slurry was coated on RDE and 20 µl on RRDE to obtain ~ 0.15mg/cm^2, which is in comparison with the cobalt metal content.

Koutecky-Levich (K-L) plots were obtained from the K-L equation[4]

$$\frac{1}{j} = \frac{1}{j_d} + \frac{1}{j_k} + \frac{1}{j_f} \; (Eqn. S1)$$

where j is the measured current density, j_k is the kinetic current density, j_d is the diffusion (mass-transfer) limited current density and j_f is the film diffusion current. Here, j_f can be neglected as the amount of Nafion is significantly low and hence will not affect the limiting current density. In the laminar flow region, the diffusion current density is a function of the rotational velocity and hence the above equation may be approximated as follows:

$$\frac{1}{j} = \frac{1}{j_d} + \frac{1}{j_k} = -\frac{1}{nFkC^b} - \frac{1}{0.62nAFD^{\frac{3}{2}}\nu^{-\frac{1}{6}}C^b\omega^{\frac{1}{2}}} \; (Eqn. S2a)$$

$$j_d = 0.62nFAC^bD_{O_2}^{2/3}\nu^{-1/6}\omega^{1/2} \; (Eqn. S2b)$$

where F is the Faraday constant (96485 C mol^{-1}), k is the rate constant for O_2 reduction, n is the number of electrons, A is the area of the electrode, C^b is the concentration of O_2 in the bulk (1.22×10^{-6} mol mL^{-1}), D is the diffusion coefficient of O_2 (1.93×10^{-5} cm^{2}s^{-1}), ν is the kinematic viscosity of solution (0.01 cm^{2}s^{-1}), and ω is the rotating speed (rad s^{-1}). From the K−L equation, the reciprocal of square root of rotating speed ($\omega^{-1/2}$) and the reciprocal of measured current density (j^{-1}) should exhibit a linear relationship.[5] The value obtained for the kinetic current was independent of diffusion and could be used to evaluate the intrinsic activity of the catalysts. The plot of the inverse of current density ($1/j$) as a function of the inverse of the square root of the rate ($\omega^{-1/2}$), at a particular potential obtained from the hydrodynamic voltammogram, assists in the evaluation of the useful kinetic parameters such as kinetic current density (j_k), number of electron transfer (n) and rate constant for ORR (k).

Number of electron transfer and H_2O_2 yield were measured using rotating ring disk electrode (RRDE) with ring as platinum and disk as glassy carbon (0.12 cm^2), (CF: 0.41). 20 µl of sample was drop casted on disk region and nafion was added just before drying. The fraction of current due to HO^{2-} that is recorded by the ring electrode (X_{HO2-}) and the corresponding electron transfer numbers during ORR (ne^-) can be determined from the following equation.[6]

$$X_{HO_2^-} = \frac{2I_R/N}{I_D + I_R/N} \, (Eqn. S3)$$

$$n_{e^-} = \frac{4I_D}{I_D + I_R/N} \, (Eqn. S4)$$

where I_R is the ring current, I_D is the disk current, and N is the collection efficiency.

The ORR equations and equilibrium potentials (vs. SHE) in acidic and alkaline media are shown in Eqn S5-S10.

A. Alkaline media

1. $O_2 + 2H_2O + 4e^- \leftrightarrow 4OH^-$; $E^0 = 0.401$ V vs SHE --------------------- (S5)

   or,

2. (a) $O_2 + H_2O + 2e^- \leftrightarrow HO_2^- + OH^-$; $E^0 = -0.076$ V vs SHE ---------- (S6)

   followed by either further reduction through,

   (b) $HO_2^- + H_2O + 2e^- \leftrightarrow 3OH^-$; $E^0 = 0.878$ V vs SHE ---------------- (S7a)

   Or disproportionation by

   (c) $2HO_2^- \leftrightarrow 2OH^- + O_2$ --- (S7b)

B. Acidic media

1. $O_2 + 4H^+ + 4e^- \leftrightarrow 2H_2O$; $E^0 = 1.229$ V vs SHE ---------------------- (S8)

   or,

2. (a) $O_2 + 2H^+ + 2e^- \leftrightarrow H_2O_2$; $E^0 = 0.695$ V vs SHE ------------------- (S9)

   Followed by either,

   (b) $H_2O_2 + 2H^+ + 2e^- \leftrightarrow 2H_2O$; $E^0 = 1.776$ V vs SHE --------------- (S10a) or,

(c) $2H_2O_2 \leftrightarrow 2H_2O + O_2$ -- (S10b)

Tables

Table S1. Elementral analyses of the electrocatalysts through various techniques

	Compound	C (conc. a.u.)	N (conc. a.u.)	H (conc. a.u.)	Co conc. a.u.)	Method
1	TZA-COF	47.35	25.56	4.33	-	CHNS
2	COF-GO-10	46.46	23.04	3.45	-	
3	COF-GO-Co	78.92	14.96		6.13	FESEM-EDS
4	Co@NC-600	83.06	4.55		12.39	
5	Co@NC-600-After ORR	87.13	2.46		10.41	

Table S2. I_D/I_G rations of the electrocatalysts as obtained from the Raman spectra

	Compound	I_G (1600 cm^{-1})	I_D (1360 cm^{-1})	I_D/I_G
1	TZA-COF	-	-	-
2	COF-GO-10	72	75	1.03
3	COF-GO-Co	22	20	0.9
4	Co@NC-600	343	404	1.17

Table S3. Comparative ORR activity table with recently reported benchmark ctalysts.

Sl No.	Catalyst	E_{onset} vs RHE	$E_{1/2}$ vs RHE	Tafel slope (mv/dec)		n_{e-}	% H_2O_2 yield	Remarks	Reference
		Initial	*Initial*	low current density	High current density		@ 0.75V		
1.	**Co-NC @ 600°C**	0.94	0.835	66.5	140	3.94	0.8		This work
2.	**COF-GO(10)-Co**	0.88	0.77	76.9	178	3.8	4.3		
3.	**COF-GO(10)**	0.88	0.81	56	134	3	30.5		
4.	**TZA-COF**	0.86	0.76	67.05	124	2.8	35.2		
5.	$Co_{3.5}C_{83}N_5O_{13}H_{59}$ (Co based coordination compound)	0.8	0.65	98		3.45	26	80% retention of current density after CA @ 25 hrs	7
6.	CoOOH-PPy-BP (polypyrrole-modified carbon-supported cobalt oxyhydroxide)	0.83	0.69			3.77 (2+2)	7 to 19		8
7.	CoO_x - 800°C (Co/CoO/Co_3O4 heterojunction encapsulated in a porous carbon framework)	0.1V vs Ag/AgCl	0.5V vs Ag/AgCl			3.9	-	Stable upto 1000 CV cycles	9
8.	Co–N–C (0.5% Co in the catalyst precursor)	0.85	0.7	65			5		10
9.	Pd/rGO	0.93	0.73					Negligible reduction in $E_{1/2}$ value	11
10.	Au/rGO	0.86	0.7			3.9		95% retention of j under 0.80 V for 13.9 h	12
11.	$FePd_3$/rGO	0.93	0.75			3.7			13
12.	Pd/MWCNT	0.96	0.81	74	130	4			14
13.	Ag@Pd/MWCNTs	0.83	0.72			2.87		50% retention of specific current under 0.82 V for 0.5 h	15
14.	Au@Pd/rGO	0.9	0.7			4		10 mV loss of $E_{1/2}$ after 1000 cycles from 1.01 to 0.22 V	16
15.	Ag/CNT	0.85	0.74	65		3.9			17

16.	Ag/GO/C	0.84	0.7						18
17.	Ag/GO-S-$(CH_2)_2$–SH	0.88	0.67	120					19
18.	Fe/Fe_3C/N/C	0.98	0.87			3.85	15	62% retention of j under 0.81 V for 5.6 h	20
19.	Fe/$Fe_{2.5}C$/N/C	0.9	0.72			3.85	6	42 mV penalty of $E_{1/2}$ after 5000 cycles from 1.0 to 0.6 V	21
20.	FeN/Fe_2N/NGR	0.92	0.78	59		4		91% retention of j under 0.71 V for 5.6 h	22
21.	Co/N/C	0.9	0.77			3.98	2.5	9 mV penalty of E1/2 after 10 000 cycles from 1.0 to 0.6 V	23
22.	Co/N/C	0.84	0.65			3.8		90% retention of j for 2.8 h	24
23.	Co/N/rGO	0.83	-----			3.97		80% retention of j under 0.66 V for 6 h	25
24.	S doped Fe-N-graphene	0.85	0.66			3.57		15mV penality after 10000 cycles in $E_{1/2}$	26
25.	Fe -encapsulated NDPCs (HBY-COF-900)	0.84	0.73			3.7	14	0.5M H_2SO_4. FeN_4 are the active sites	27
26.	CoAl-LDH@ZIF-67	0.87	0.675	63	115	3.9	<10%	N–C, Co–N–C as active sites	28
27.	Fe-N-C catalyst (from polymers)	0.83	0.72					Fe-N-C as active sites	29
28.	Fe–N–C (precursor method)	0.82	0.72			4e to 2e	~11%	Fe-N-C as active sites	30
ONLY COF BASED MATERIALS									
29.	**CTF/CP**	0.38	0.22					In 0.5M H_2SO_4. MeOH tolerant	31
30.	**Pt-CTF/CP**	0.82	0.6						31
31.	**COP-P-SO3H**	0.65	0.58	82.4				0.1M KOH	32
32.	**COP-P-SO_3-Co-rGO**	0.81	0.72	67.4					32
33.	**TAPT–DHTA–COF1000**	−0.12V vs Ag/AgCl	-0.29V vs Ag/AgCl	190		3.26-3.68	16-37	0.1M KOH	33
34.	**PA@TAPT–DHTA–COF1000**	-0.02V vs Ag/AgCl	--0.19V vs Ag/AgCl	140		3.60-3.98	12-20	0.1M KOH	33
35.	**Naphthalene-Based COF**	0.82	0.74	110.8		2.5-3.0	60-40	0.1M KOH	34, 35

Table S4. EIS (Nyquist Plot) fitting parameters. All the EIS spectra were recorded at the half-wave potential of the samples at 1600 rpm in O_2 purged 0.5M KOH.

Sample	R1	R2	C2	Q2	a2	R3	C3	Q3	a3	$\chi^2/\lvert Z\rvert$
	Ohm	Ohm	F	F.s$^{(a-1)}$		Ohm	F	F.s$^{(a-1)}$		
Co@NC-600	89.74	122.4	0.01505	10.51 x 10^{-21}	0.4123	148.6	-89.76 x 10^{-18}	2.125 x 10^{-3}	0.6825	0.023
Co@NC-700	84.23	145.7	2.209 x x10^{-18}	1.231 x 10^{-3}	0.7147	265.7	0.454 x 10^{-30}	6.097 x 10^{-3}	1	0.029
Co@NC-800	64.52	219.8	5.878 x 10^{-3}	37.23 x 10^{-132}	0	358.3	0.3348 x 10^{-18}	0.4419 x 10^{-3}	0.7709	0.03
Co@NC-700-Ethched	100.8	141.9	0.02688	0.474 x 10^{-18}	0	165.3	-15.32 x 10^{-9}	0.601 x 10^{-3}	0.7862	0.027
NC@-600	63.95	488.8	58.68 x 10^{-6}	0.231 x 10^{-3}	0.6653	214.1	4.034 x 10^{-3}	0.4608 x 10^{-3}	1	0.05
TZA-COF	80.89	382.5	7.633 x 10^{-18}	1.459 x 10^{-3}	0.7596	154	0.4059 x 10^{-3}	3.745 x 10^{-18}	1	0.01

Table S5. EIS-Bode plot analysis for different samples. All the EIS spectra were recorded at the half-wave potential of the samples at 1600 rpm in O_2 purged 0.5M KOH.

	Sample	**Phase**		**Freq**		**-Im Z**		**Freq**	
		L.F.	M.F.	L.F.	M.F.	L.F.	M.F.	L.F.	M.F.
		Deg		*Hz*		*Ohm*		*Hz*	
1.	Co@NC-600	19	17.6	0.18	1.78	86	48	0.12	1.46
2.	Co@NC-700	26	20	0.21	3.16	143.4	54.5	0.12	2.14
3.	Co@NC-800	20	35.5	0.26	4.64	159.2	140.7	0.178	1.77
4.	Co@NC-700-Ethched	13.3	19	0.056	3.8	76.2	64	0.047	2.14
5.	NC@-600	17	43.7	0.26	8.24	172	196	0.26	2.6
6.	TZA-COF	21	37	0.38	3.8	155	152	0.38	1.48
7.	COF-GO(10)	23	40	0.15	3.16	130	88	0.12	1.21
8.	COF-GO(20)	30	26	12	144	294		2.14	
9.	COF-GO(10)-Co	56		2.14		266		0.56	

Figures

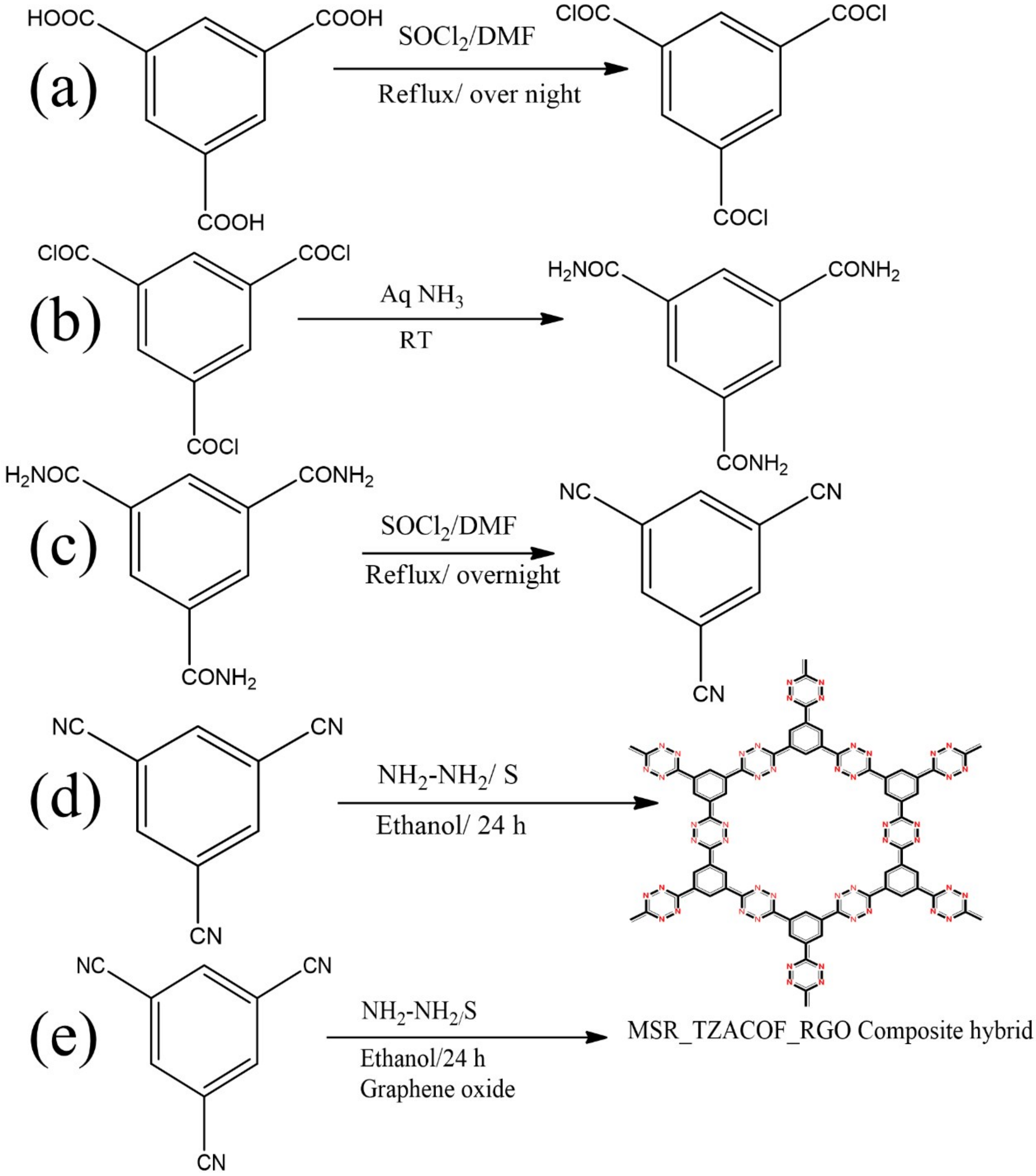

Scheme S1. Reaction conditions for ligand (BzCN), TZA-COF and COF-rGO composites.

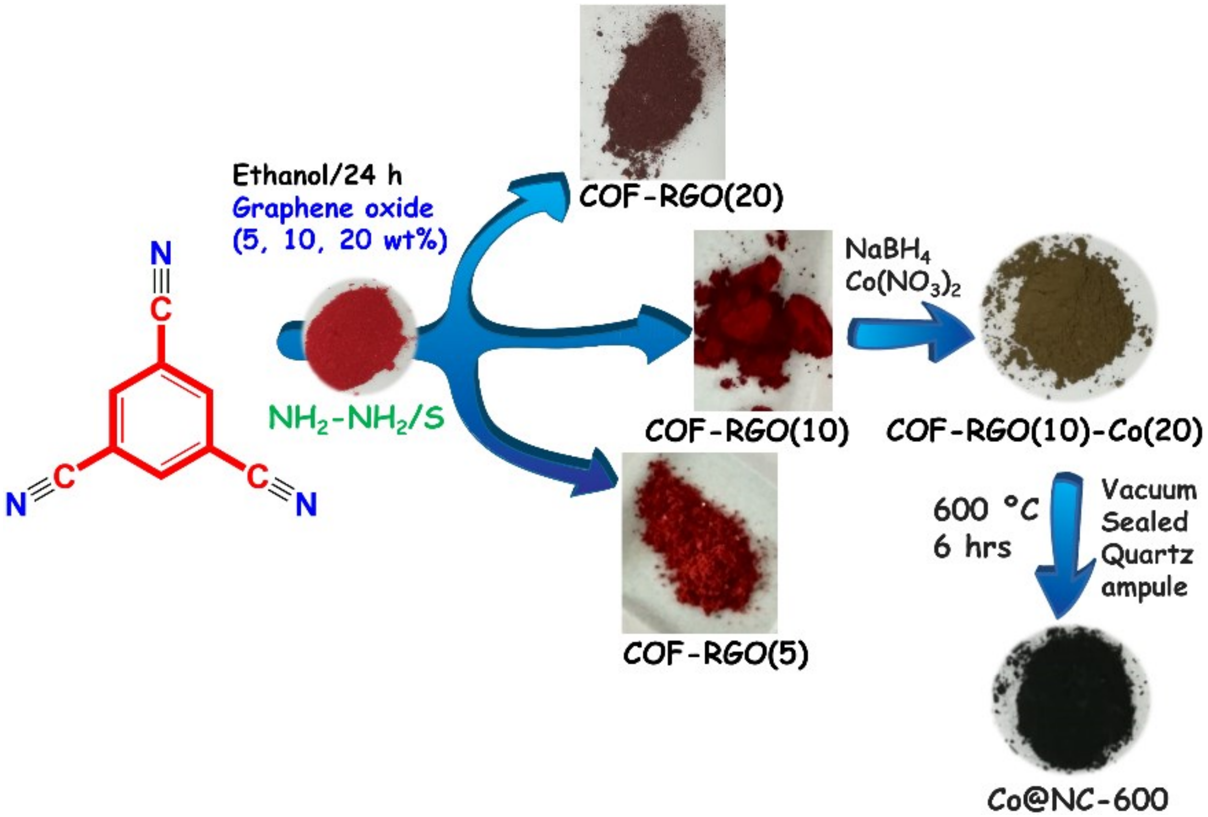

Scheme S2. Synthetic scheme and colours of the **COF-rGO** hybrids and Co-derived electrocatalysts.

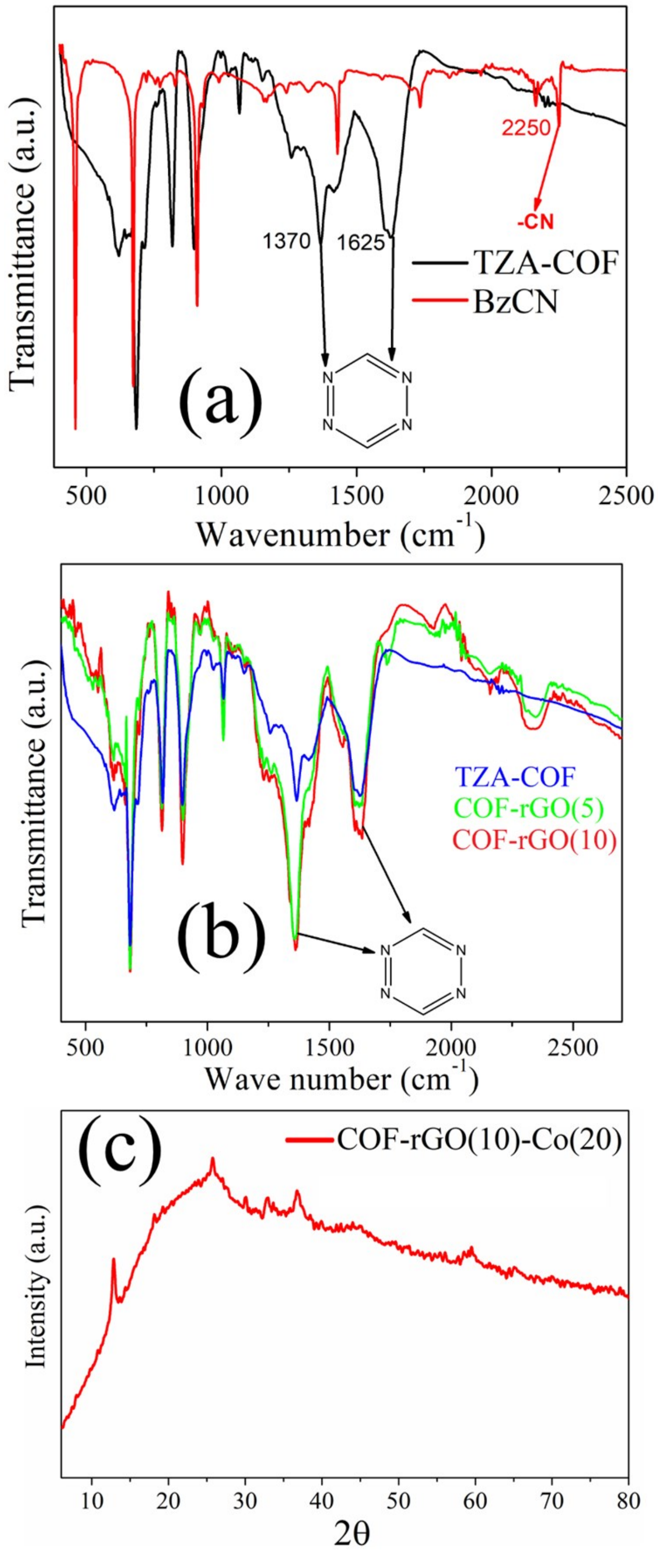

Figure S1. Structural characterization of **TZA-COF** and derived electrocatalysts. (a) IR spectra of the ligand and COF, showing the transformation of the BzCN ligand with disappearance of the -C≡N stretching frequency, (b) IR spectra of the **TZA-COF** compared to **COF-rGO** composites with different wt% of rGO and (c) PXRD pattern of **COF-rGO(10)-Co(20) hybrid**.

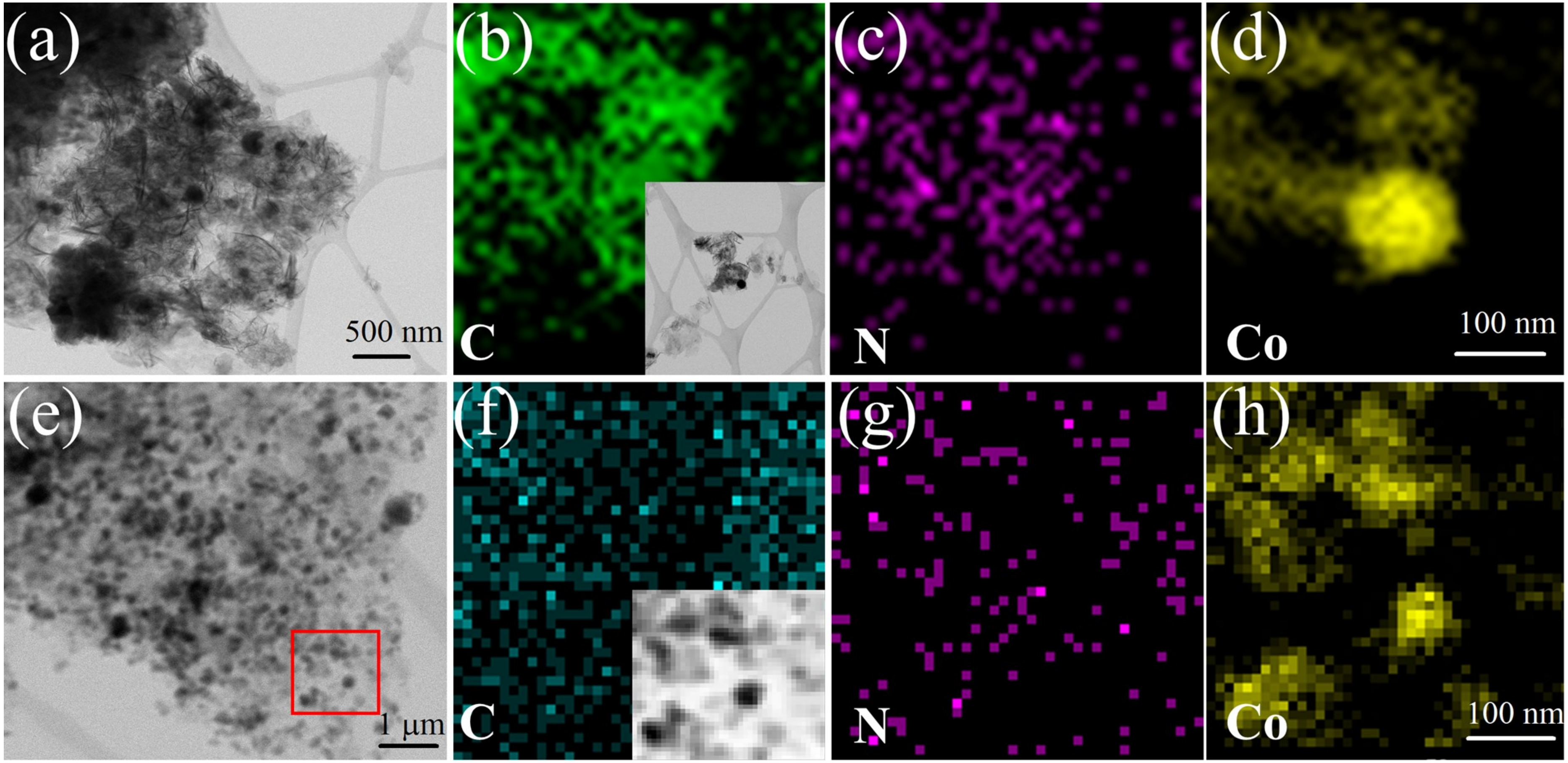

Figure S2. TEM images and elemental colour mapping of (a-d) **COF-rGO-Co** and (e-h) **Co@NC-600**.

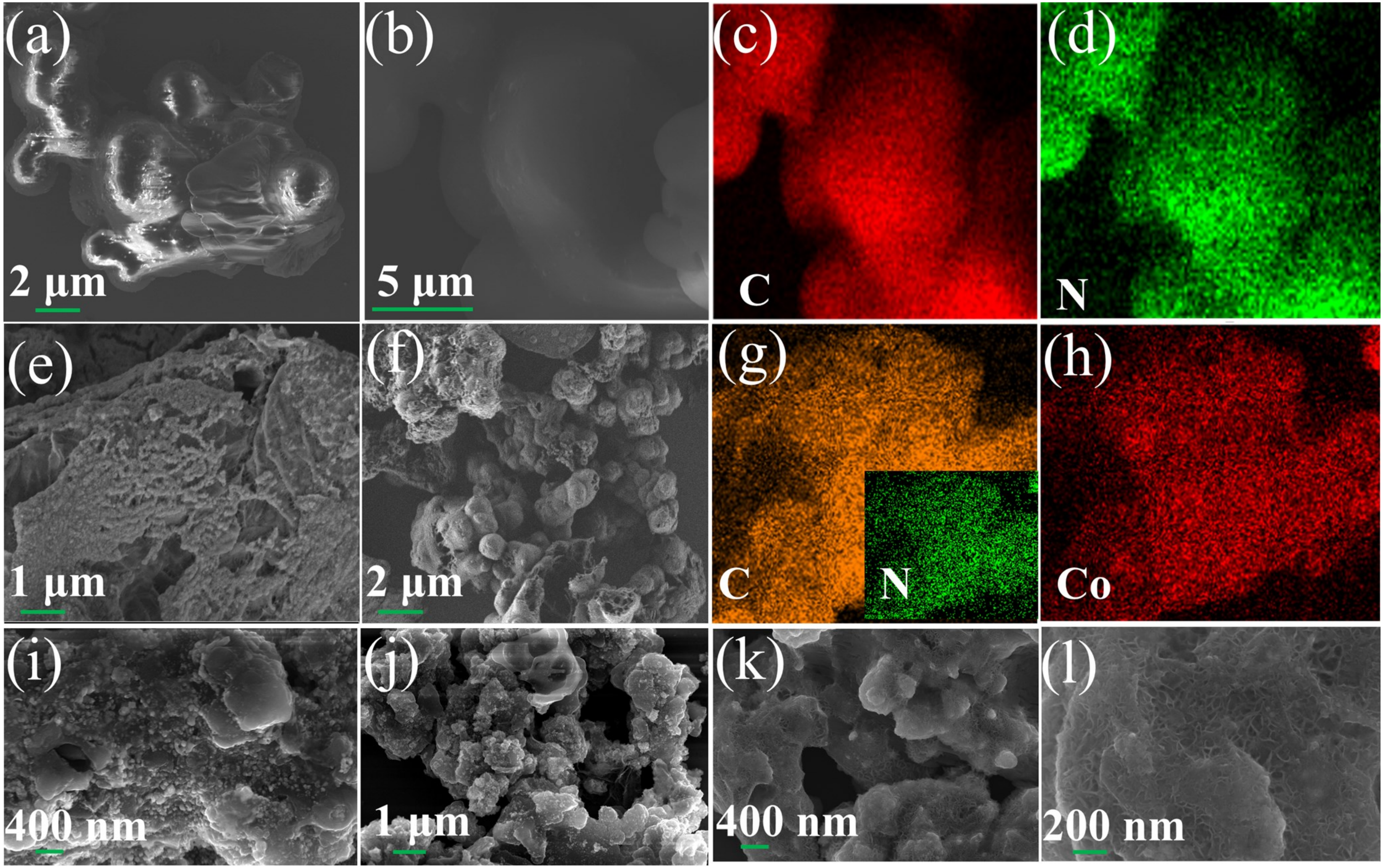

Figure S3. SEM images and elemental colour mapping of (a-d) **COF-rGO**, (e-h) **COF-rGO-Co** and (i-l) **Co@NC-600**.

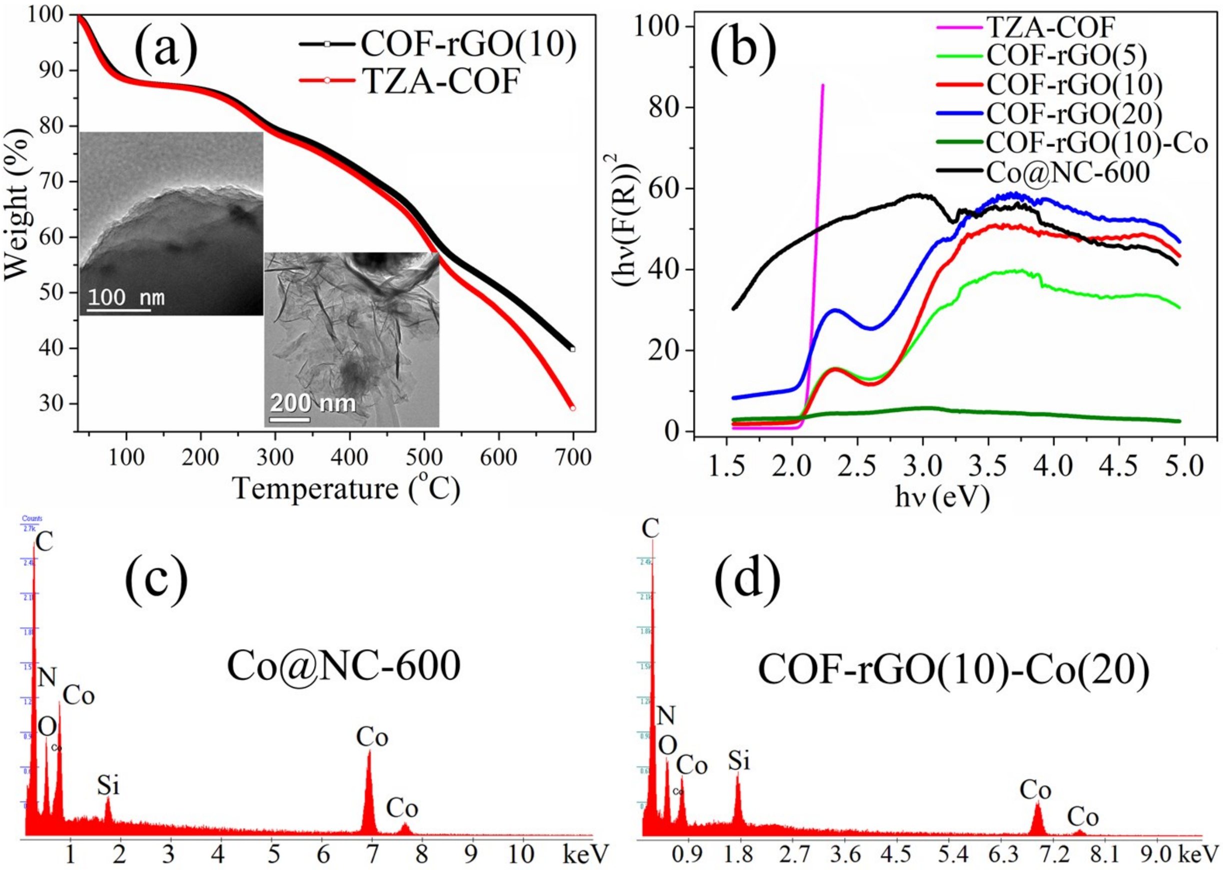

Figure S4. (a) TGA of **TZA-COF** & **COF-rGO(10)** with the TEM images of the bare COF and GOF-rGO composite in the inset, (b) K-M function plots of the catalysts obtained from solid state UV-Vis spectra illustrating the values and nature of optical band gap, and EDS spectra of (c) **Co@NC-600** and (d) **COF-rGO(10)-Co(20)**.

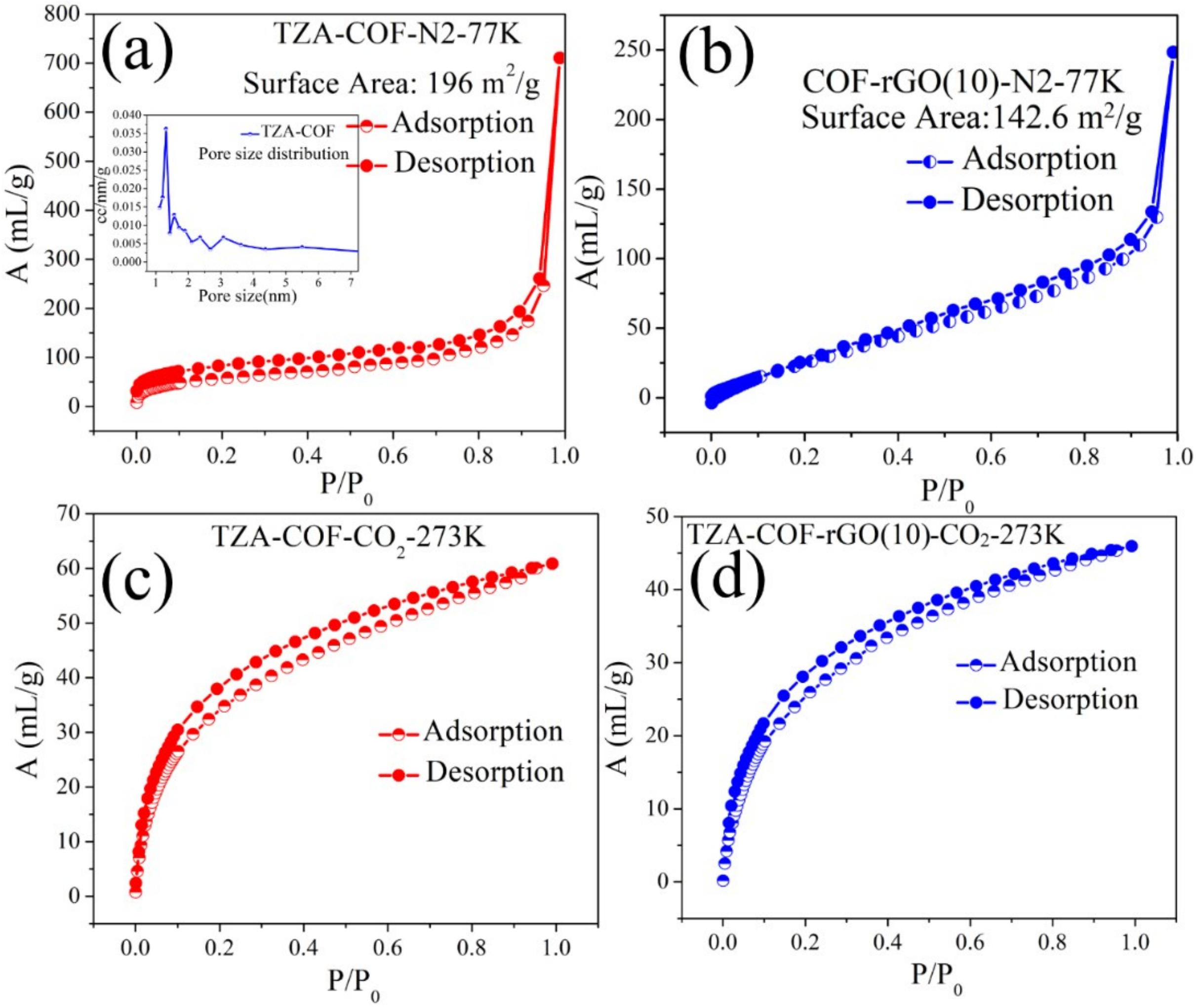

Figure S5. N_2 and CO_2 adsorption isotherms. (a) N_2 adsorption (77 K) isotherm with the pore size distribution of **TZA-COF** showing a typical type II behaviour, (b) N_2 adsorption (77 K) isotherm of **TZA-COF-rGO(10).** and CO_2 adsorption isotherms (@ 273 K) of (c) **TZA-COF** and (d) **TZA-COF-rGO(10)**.

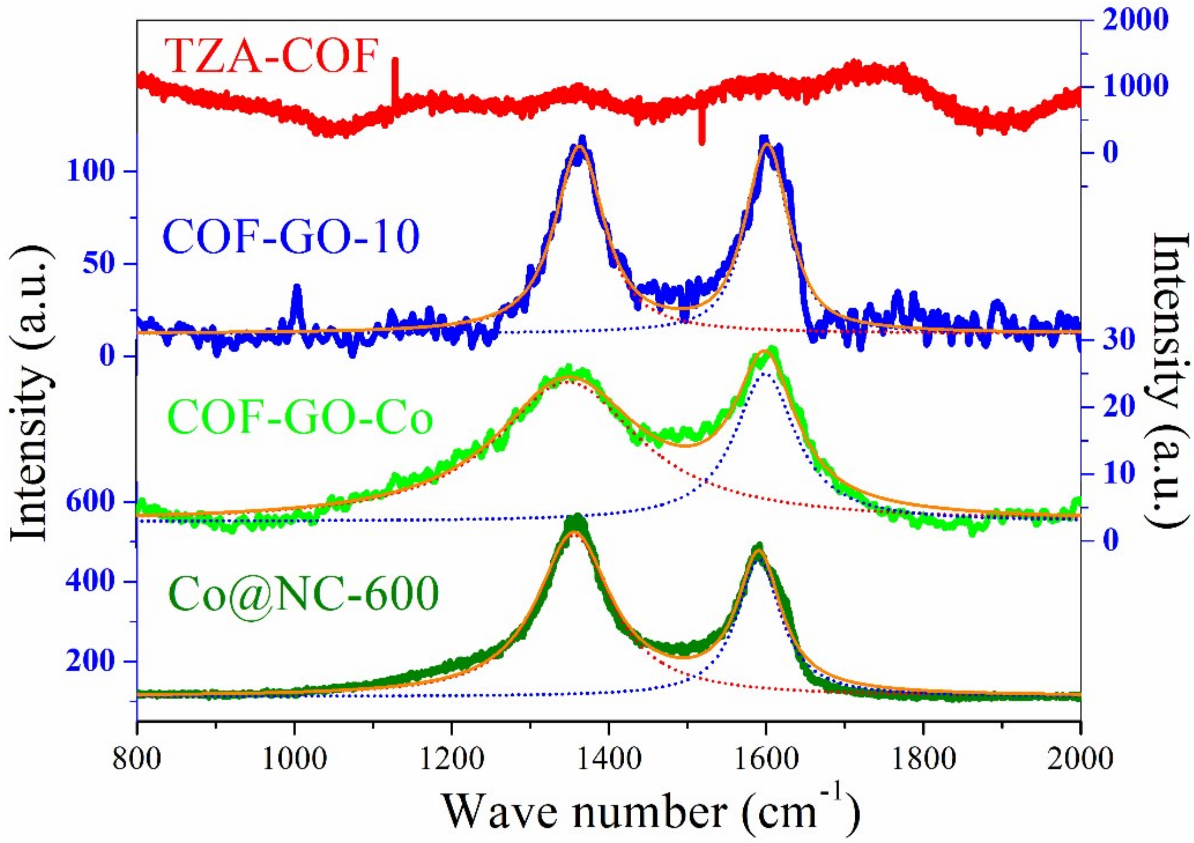

Figure S6. Raman spectra of the electrocatalysts showing the I_D/I_G bands.

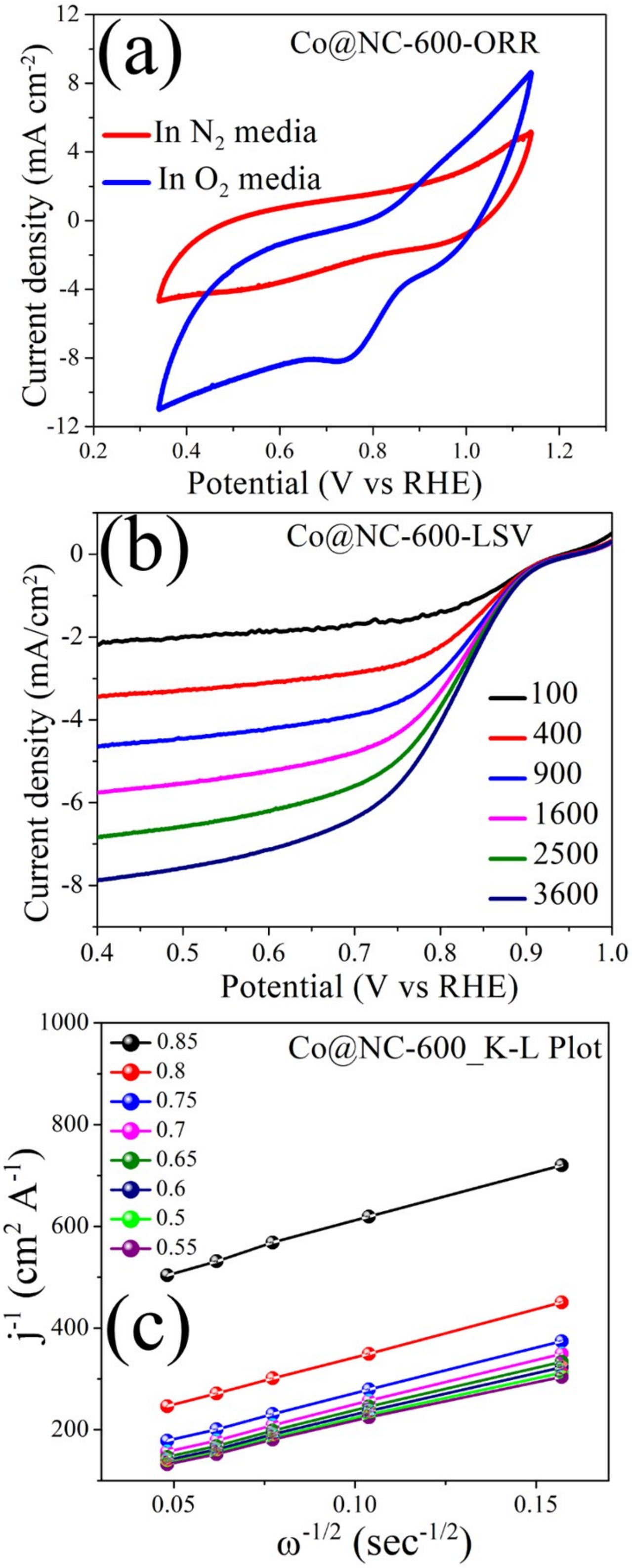

Figure S7. Electrochemical ORR activity the catalysts studied in O_2/N_2 saturated 0.1M KOH using rotating disk electrode (RDE) at a scan rate of 5 mV/s. (a) CV curves of **Co@NC-600** in N_2 and O_2 saturated electrolyte demonstrating the oxygen reduction peak, (b) ORR LSVs of **Co@NC-600** with varying rotation speeds, (c) K-L plots of **Co@NC-600** at different potentials, linearity and parallelism of which signifies the uniformity in the electron reduction process in the catalyst over a wide potential range.

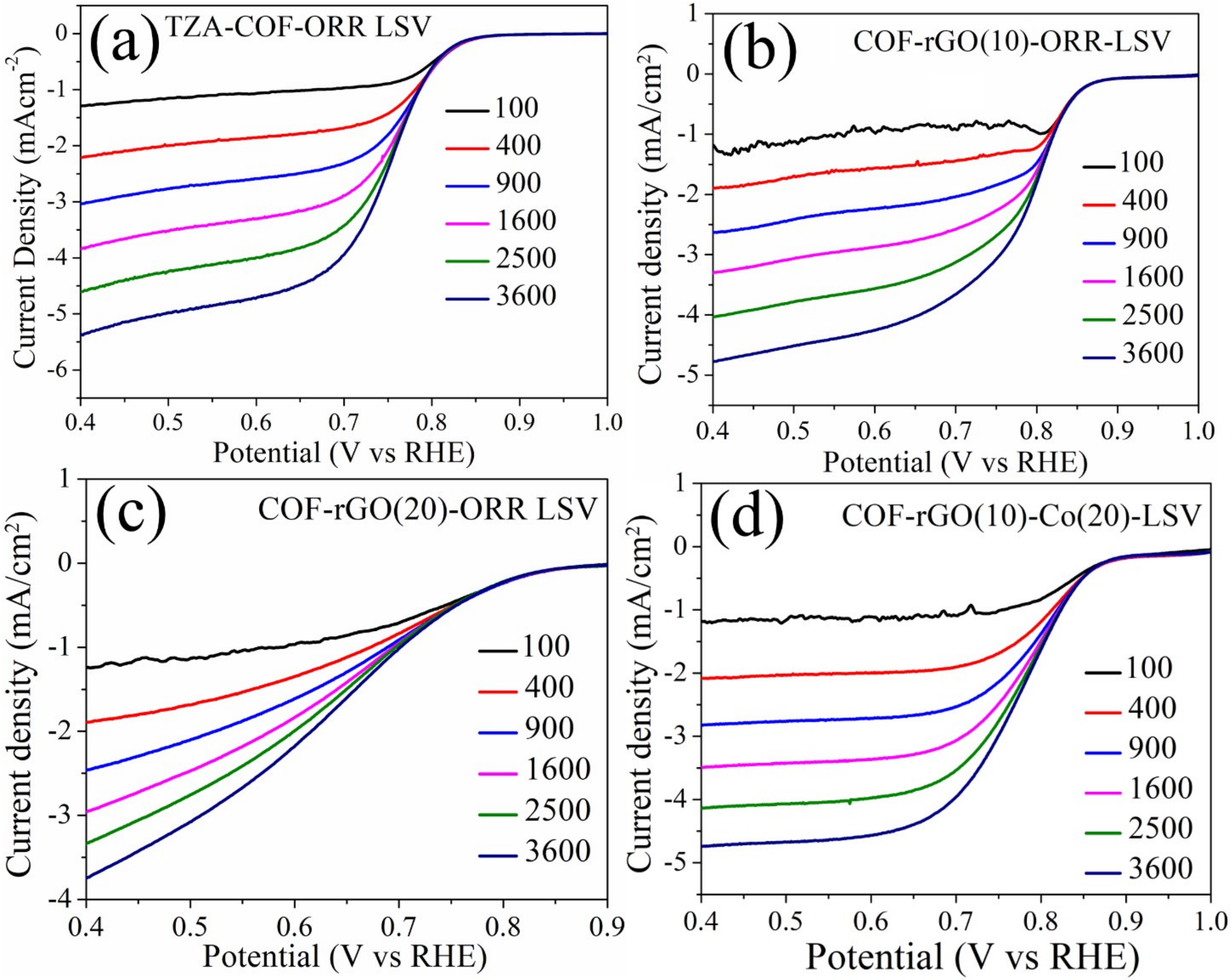

Figure S8. LSVs at different scan rates for ORR in 0.1M KOH of (a) **TZA-COF**, (b) **COF-rGO(10)**, (c) **COF-rGO(20)** and (d) **COF-rGO(10)-Co(20)**.

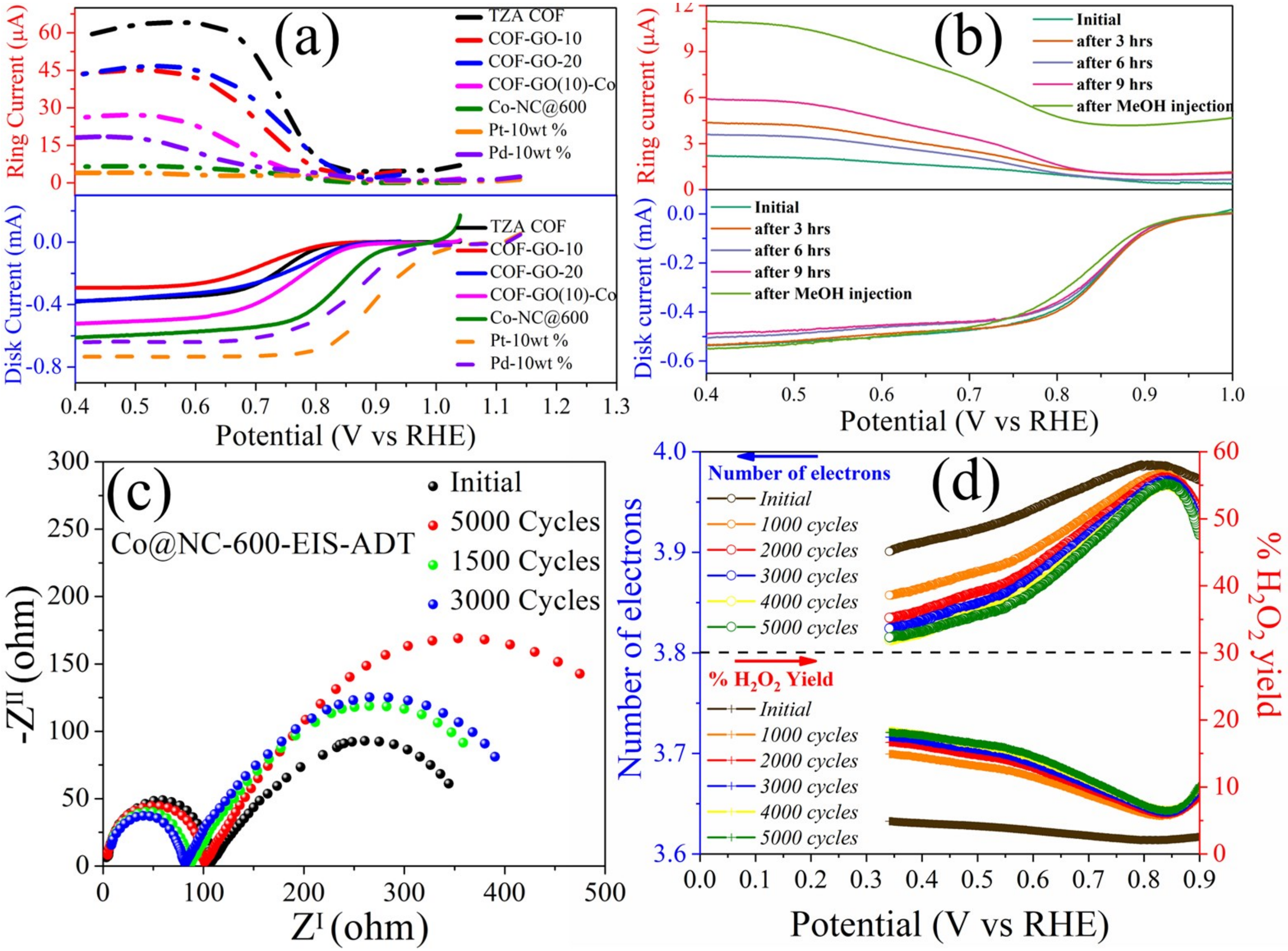

Figure S9. (a) Ring and disc currents of the electrocatalysts during ORR obtained from RRDE measurements, (b) Ring and disc currents of **Co@NC-600** at different stages of stability test (CA) as obtained from RRDE measurements, (c) Nyquist plots from EIS studies on **Co@NC-600** after different ADT cycles and (d) n_{e^-} and H_2O_2 % plots of **Co@NC-600** in the entire ORR potential range after different ADT cycles.

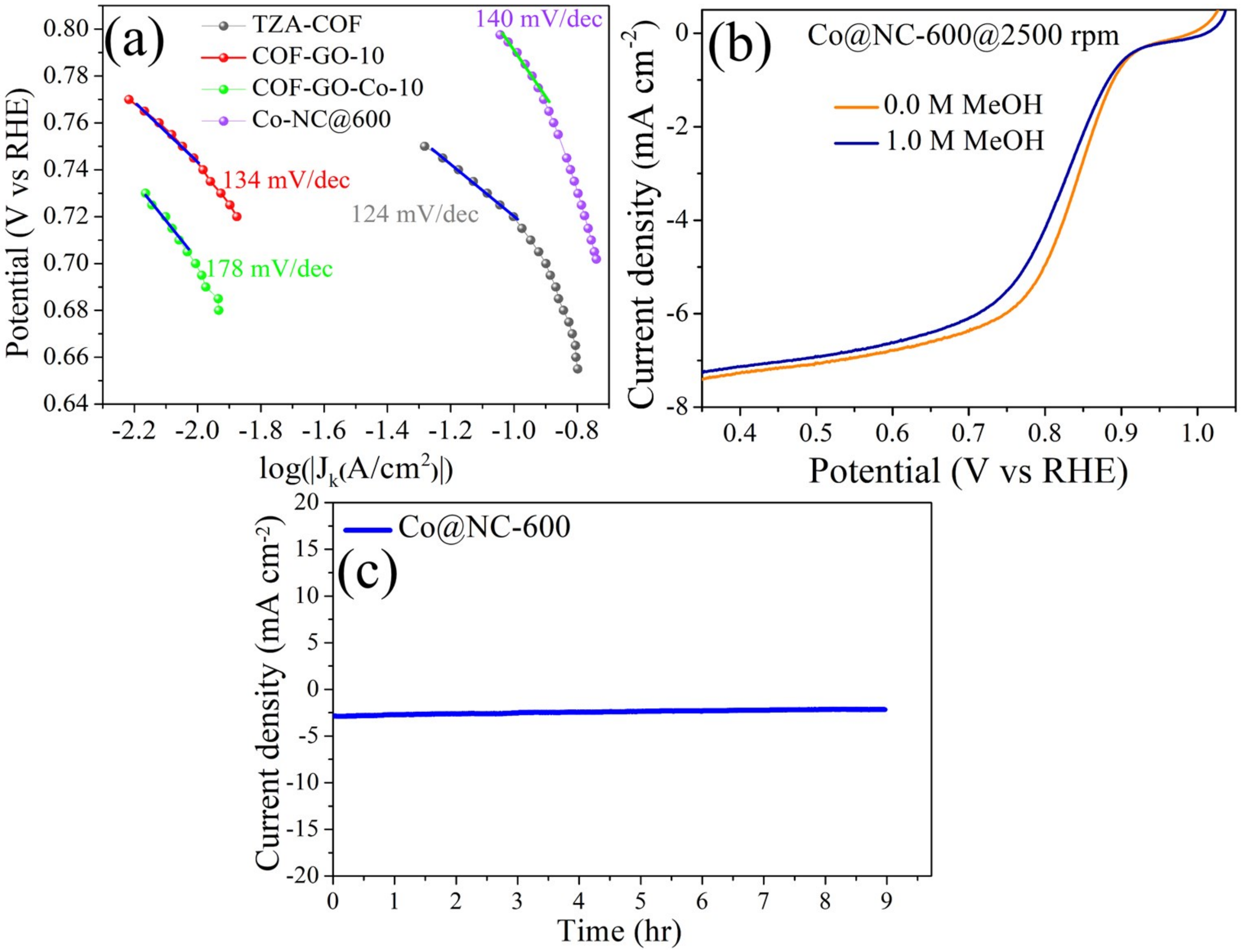

Figures S10. (a) Tafel plots of the catalysts during ORR at higher overpotential region, (b) MeOH tolerance test, showing comparative LSVs with and without MeOH in the electrolyte (1 M), and (c) 9 h chronoamperometric stability at $E_{1/2}$ of **Co@NC-600** demonstrating the exceptional stability of the electrocatalyst.

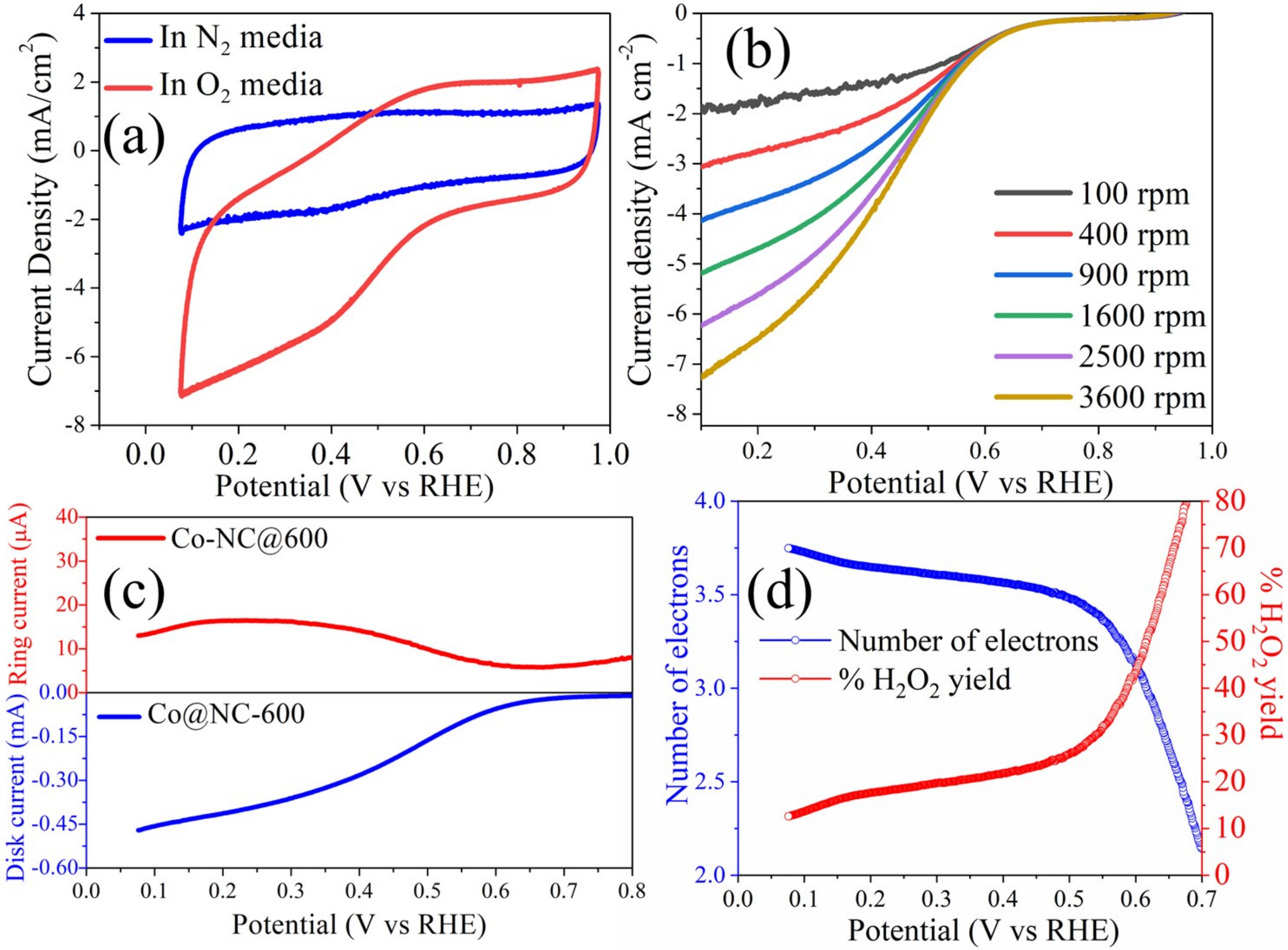

Figure S11. ORR activity of **Co@NC-600** in acidic electrolyte (0.1M $HClO_4$). (a) CV curves in N_2 and O_2 saturated electrolyte, (b) LSVs at a scan rate of 5 mV/s at different rpm, (c) ring and disc currents in RRDE measurements and (d) n_{e^-} and H_2O_2 % plots in the entire ORR potential range.

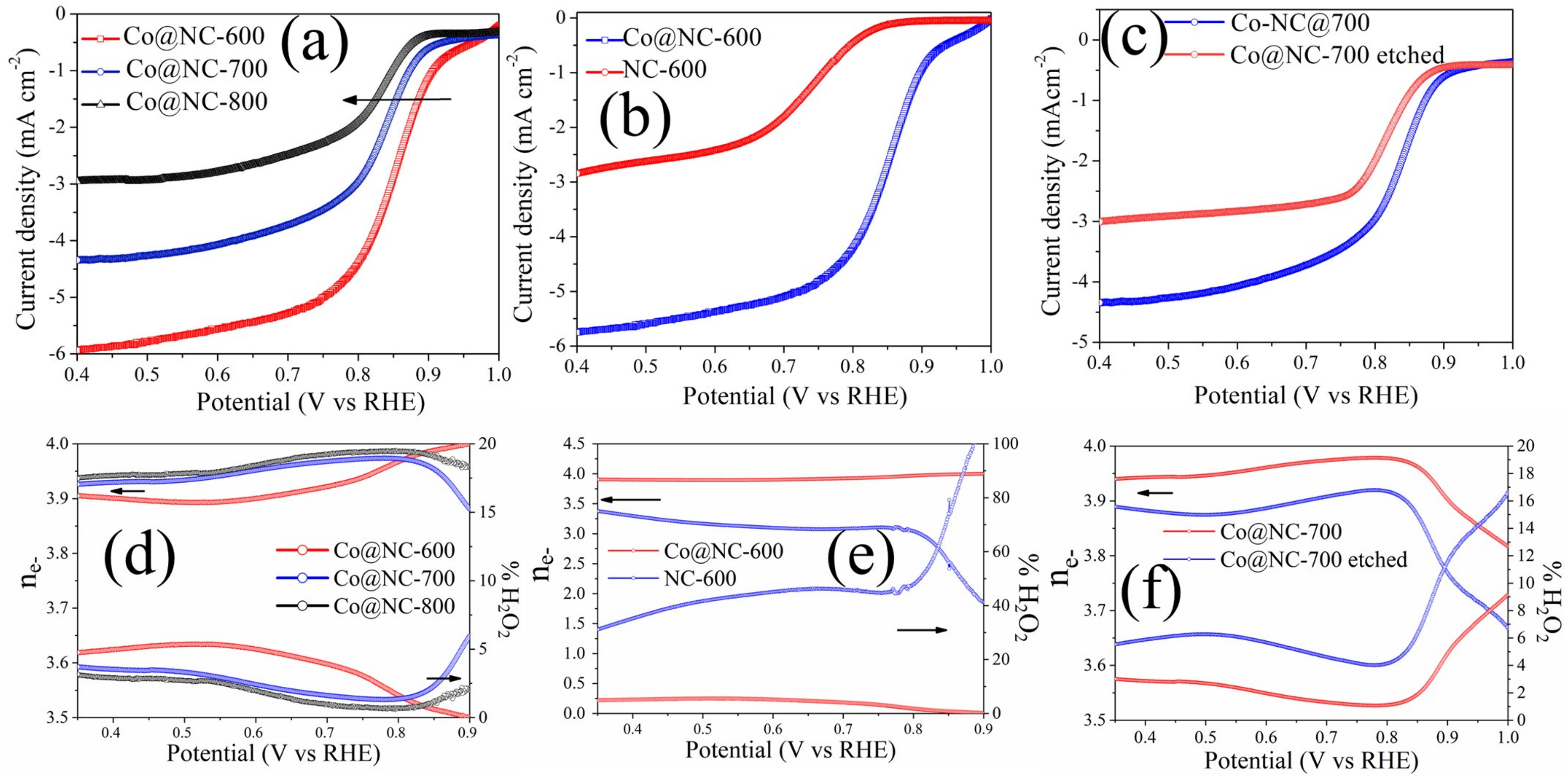

Figure S12. Comparison of electrocatalytic ORR activity across different controlled variants of the **CO@NC-600** catalyst. (a & d) LSV curves and n_{e-}/H_2O_2 % for Co@NC annealed at 600, 700 and 800 ºC, (b & e) LSV curves and n_{e-}/H_2O_2 % for **Co@NC-600** & **NC-600** catalysts, and (c & f) LSV curves and n_{e-}/H_2O_2 % for **Co@NC-700** and **Co@NC-700**-etched samples.

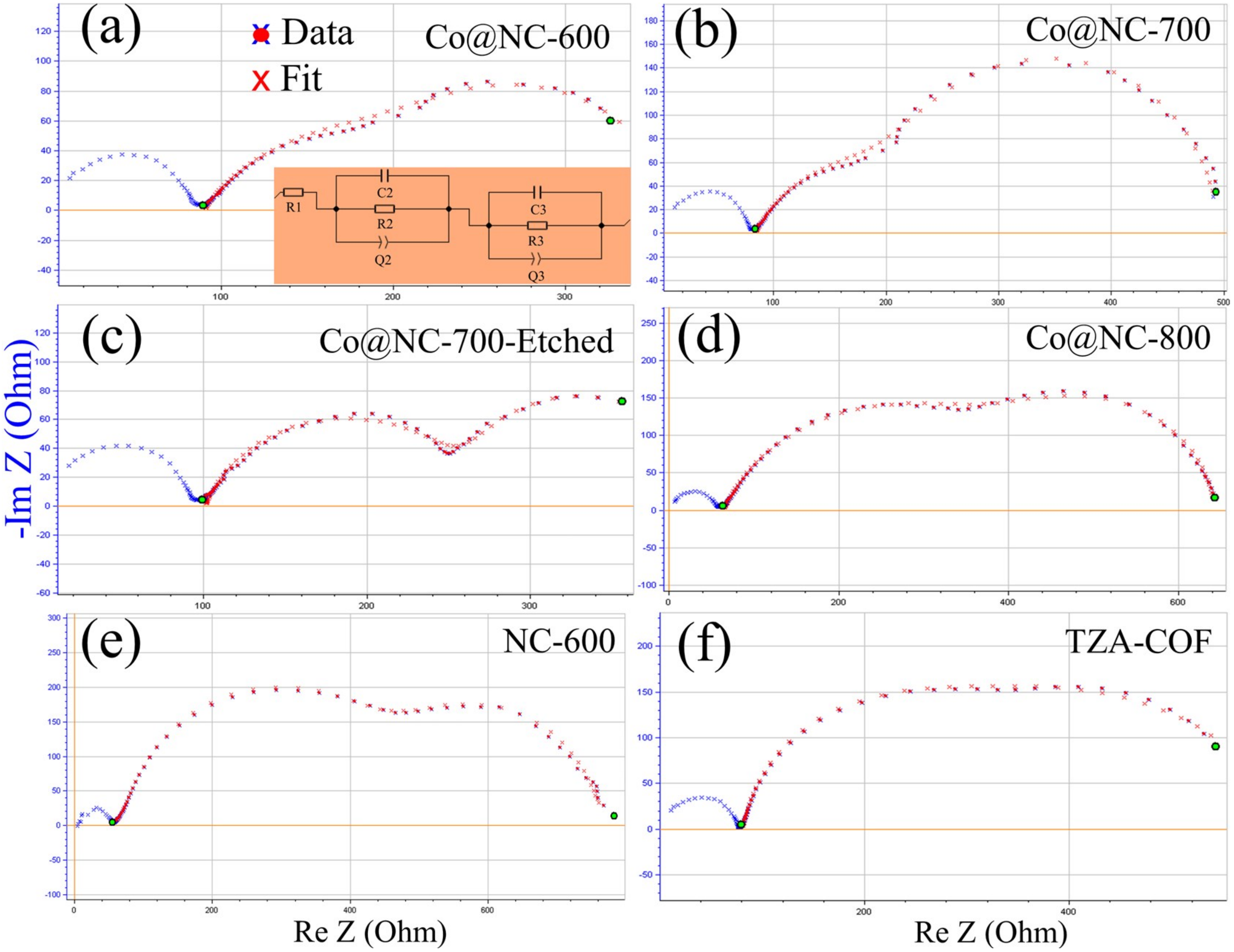

Figure S13. Fitting of the EIS Nyquist plots for different controlled variants of **Co@NC-600** catalysts.

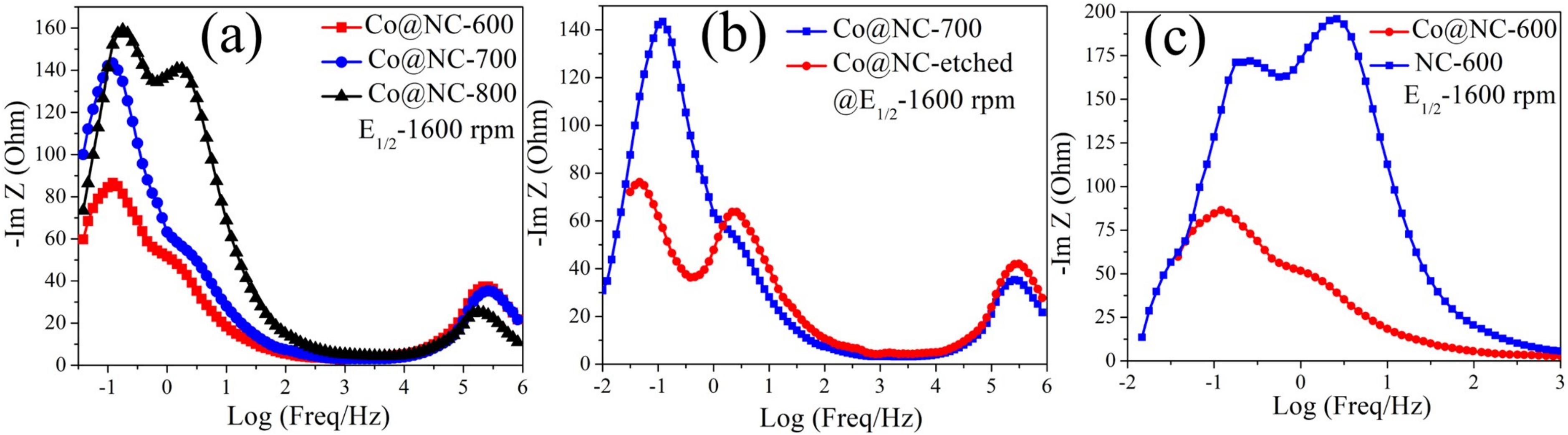

Figure S14. Comparison of electrocatalytic EIS Bode plots (-Im Z vs Log Freq) at half-wave potentials @ 1600 rpm across different controlled variants of the **CO@NC-600** catalyst. (a) Co@NC annealed at 600, 700 and 800 ºC, (b) **Co@NC-600** & **NC-600** catalysts, and (c) **Co@NC-700** and **Co@NC-700**-etched samples.

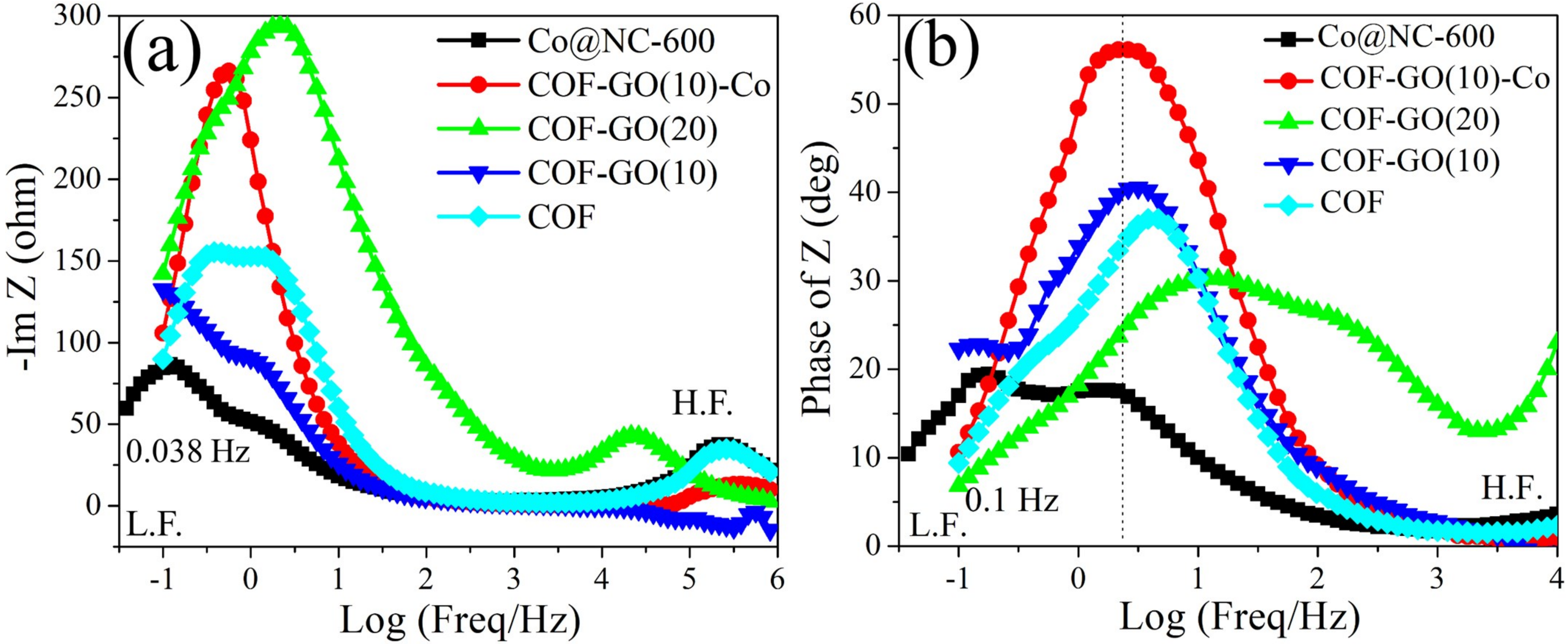

Figure S15. Comparison of electrocatalytic EIS Bode plots at half-wave potentials @ 1600 rpm at different stages of structural engineering with respect to (a) the imaginary part of Z and (b) phase of Z.

References

1. P. Katekomol, J. Roeser, M. Bojdys, J. Weber and A. Thomas, *Chem. Mater.*, 2013, **25**, 1542.
2. D.-S. Zhang, Z. Chang, Y.-B. Lv, T.-L. Hu and X.-H. Bu, *RSC Adv.*, 2012, **2**, 408.
3. N. I. Zaaba, K. L. Foo, U. Hashim, S. J. Tan, W.-W. Liu and C. H. Voon, *Procedia Engineering*, 2017, **184**, 469.
4. S. Xu, Y. Kim, D. Higgins, M. Yusuf, T. F. Jaramillo and F. B. Prinz, *Electrochim. Acta*, 2017, **255**, 99.
5. X. Min, Y. Chen and M. W. Kanan, *Phys. Chem. Chem. Phys.*, 2014, **16**, 13601.
6. X. Ge, A. Sumboja, D. Wuu, T. An, B. Li, F. W. T. Goh, T. S. A. Hor, Y. Zong and Z. Liu, *ACS Catal.*, 2015, **5**, 4643.
7. P. Mani, A. Sheelam, S. Das, G. Wang, V. K. Ramani, K. Ramanujam, S. K. Pati and S. Mandal, *ACS Omega*, 2018, **3**, 3830.
8. J. Wang, L. X. Lin, Y. He, H. Y. Qin, S. Yan, K. Yang, A. G. Li and J. B. Liu, *Electrochim. Acta*, 2017, **254**, 72.
9. X. C. Li, F. S. She, D. Shen, C. P. Liu, L. H. Chen, Y. Li, Z. Deng, Z. H. Chen and H. E. Wang, *RSC Adv.*, 2018, **8**, 28625.
10. A. Zitolo, N. Ranjbar-Sahraie, T. Mineva, J. Li, Q. Jia, S. Stamatin, G. F. Harrington, S. M. Lyth, P. Krtil, S. Mukerjee, E. Fonda and F. Jaouen, *Nat. Commun.*, 2017, **8**, 957.
11. Y.-X. Huang, J.-F. Xie, X. Zhang, L. Xiong and H.-Q. Yu, *ACS Appl. Mater. Interfaces*, 2014, **6**, 15795.
12. M. Govindhan and A. C. Chen, *J. Power Sources*, 2015, **274**, 928.
13. H. Yin, S. Liu, C. Zhang, J. Bao, Y. Zheng, M. Han and Z. Dai, *ACS Appl. Mater. Interfaces*, 2014, **6**, 2086.
14. K. Jukk, N. Alexeyeva, P. Ritslaid, J. Kozlova, V. Sammelselg and K. Tammeveski, *Electrocatalysis*, 2013, **4**, 42.
15. R. C. Sekol, X. K. Li, P. Cohen, G. Doubek, M. Carmo and A. D. Taylor, *Appl. Catal. B*, 2013, **138**, 285.
16. S. S. Li, A. J. Wang, Y. Y. Hu, K. M. Fang, J. R. Chen and J. J. Feng, *J. Mater. Chem. A*, 2014, **2**, 18177.
17. A. Fazil and R. Chetty, *Electroanalysis*, 2014, **26**, 2380.
18. L. Z. Yuan, L. H. Jiang, J. Liu, Z. X. Xia, S. L. Wang and G. Q. Sun, *Electrochim. Acta*, 2014, **135**, 168.
19. K. Lee, M. S. Ahmed and S. Jeon, *J. Electrochem. Soc.*, 2015, **162**, F1.
20. J. S. Lee, G. S. Park, S. T. Kim, M. L. Liu and J. Cho, *Angew. Chem. Int. Ed.*, 2013, **52**, 1026.
21. L. Z. Gu, L. H. Jiang, J. T. Jin, J. Liu and G. Q. Sun, *Carbon*, 2015, **82**, 572.
22. H. Yin, C. Z. Zhang, F. Liu and Y. L. Hou, *Adv. Funct. Mater.*, 2014, **24**, 2930.
23. H. W. Liang, W. Wei, Z. S. Wu, X. L. Feng and K. Mullen, *J. Am. Chem. Soc.*, 2013, **135**, 16002.
24. H. Wang, X. J. Bo, A. X. Wang and L. P. Guo, *Electrochem. Commun.*, 2013, **36**, 75.
25. B. Zheng, J. Wang, F. B. Wang and X. H. Xia, *J. Mater. Chem. A*, 2014, **2**, 9079.
26. S. Oh, J. Kim, M. Kim, D. Nam, J. Park, E. Cho and H. Kwon, *J. Mater. Chem. A*, 2016, **4**, 14400.
27. S.-B. Ren, J. Wang and X.-H. Xia, *ACS Appl. Mater. Interfaces*, 2016, **8**, 25875.
28. Z. H. Li, M. F. Shao, L. Zhou, R. K. Zhang, C. Zhang, M. Wei, D. G. Evans and X. Duan, *Adv. Mater.*, 2016, **28**, 2337.
29. Y. S. Zhu, B. S. Zhang, Z. B. Feng and D. S. Su, *Catal. Today*, 2016, **260**, 112.
30. U. I. Kramm, A. Zana, T. Vosch, S. Fiechter, M. Arenz and D. Schmeisser, *J. Solid State Electrochem.*, 2016, **20**, 969.
31. K. Kamiya, R. Kamai, K. Hashimoto and S. Nakanishi, *Nat. Commun.*, 2014, **5**, 5040.
32. J. Guo, C.-Y. Lin, Z. Xia and Z. Xiang, *Angew. Chem. Int. Ed.*, 2018, **57**, 12567.
33. Q. Xu, Y. Tang, X. Zhang, Y. Oshima, Q. Chen and D. Jiang, *Adv. Mater.*, 2018, **30**, 1706330.
34. C. You, X. Jiang, X. Wang, Y. Hua, C. Wang, Q. Lin and S. Liao, *ACS Appl. Energy Mater.*, 2018, **1**, 161.
35. C. H. You, X. W. Jiang, L. Y. Han, X. H. Wang, Q. Lin, Y. J. Hua, C. T. Wang, X. L. Liu and S. J. Liao, *J. Mater. Chem. A*, 2017, **5**, 1742.